Probabilistic Fuzzy Image Fusion Approach for Radar Through Wall Sensing

Cher Hau Seng, Abdesselam Bouzerdoum, *Senior Member, IEEE*, Moeness G. Amin, *Fellow, IEEE*, and Son Lam Phung, *Member, IEEE*

***Abstract*— This paper addresses the problem of combining multiple radar images of the same scene to produce a more informative composite image. The proposed approach for probabilistic fuzzy logic-based image fusion automatically forms fuzzy membership functions using the Gaussian–Rayleigh mixture distribution. It fuses the input pixel values directly without requiring fuzzification and defuzzification, thereby removing the subjective nature of the existing fuzzy logic methods. In this paper, the proposed approach is applied to through-the-wall radar imaging in urban sensing and evaluated on real multi-view and polarimetric data. Experimental results show that the proposed approach yields improved image contrast and enhances target detection.**

***Index Terms*— Fuzzy logic, image fusion, through-the-wall radar imaging.**

I. Introduction

IN REMOTE sensing applications, through-the-wall radar imaging (TWRI) systems are used to detect the presence of targets behind obstacles [1]–[4]. However, due to unknown wall characteristics, multipath and clutter, the acquired radar images tend to deviate from the ground truth, which hampers target detection and localization.

During the sensing process, the same scene may be imaged from different viewing angles, using one or multiple systems. The same scene can also be imaged from the same viewing angle, but with different polarizations. Both operations are motivated by the fact that target radar cross section (RCS) contains valuable information that single view or single polarization does to provide [5], [6]. Since images acquired from different viewing angles and polarizations provide different representations of the same scene, multiple images can be combined to produce a more informative composite image, and enhance target detection and localization [7], [8].

Manuscript received January 5, 2012; revised January 6, 2013 and August 13, 2013; accepted August 13, 2013. Date of publication August 28, 2013; date of current version October 1, 2013. The work of C. H. Seng, A. Bouzerdoum, and S. L. Phung was supported in part by a grant from the Australian Research Council. The work of M. G. Amin was supported in part by Office of Naval Research under Grant N000141010455. The associate editor coordinating the review of this manuscript and approving it for publication was Prof. Brian D. Rigling.

C. H. Seng, A. Bouzerdoum, and S. L. Phung are with the School of Electrical, Computer and Telecommunications Engineering, University of Wollongong, Wollongong 2522, Australia (e-mail: aseng@uow.edu.au; a.bouzerdoum@uow.edu.au; phung@uow.edu.au).

M. G. Amin is with the Center for Advanced Communications, Villanova University, Villanova, PA 19085 USA (e-mail: moeness.amin@villanova.edu).

Color versions of one or more of the figures in this paper are available online at http://ieeexplore.ieee.org.

Digital Object Identifier 10.1109/TIP.2013.2279953

Multi-view and polarimetric imaging techniques have been successfully applied in many radar applications [9]–[11]. However, existing image fusion methods are mostly developed to fuse images from different modalities, such as between optical and infrared images [12]–[14], between Synthetic Aperture Radar (SAR) and optical images [15]–[17], and between SAR and panchromatic images [7], [8]. There have been few studies regarding the fusion of images obtained from the same scene and from the same type of sensors, which is important in TWRI. Furthermore, due to the differences in indoor and clutter scattering characteristics with other radar imaging paradigms [18], existing fusion methods such as the Discrete Wavelet Transform (DWT) and Principal Component Analysis (PCA), which are commonly used in SAR, are not directly applicable in TWRI.

To date, simple arithmetic image fusion methods have been proposed to improve TWRI [18], [19]. Additive image fusion was first introduced for TWRI in [19] to compensate for target displacements that are caused by unknown wall parameters. It was shown that the fusion of images obtained from different standoff positions reveals the exact location of the targets. The work in [18] later considered moving the antenna array around a building, and then combining the images through multiplicative fusion to improve detection and localization of indoor targets. Additive and multiplicative fusion were also used in [20], [21] to enhance a polarimetric radar by combining the images obtained in co-polarization and cross-polarization scenarios.

Although the arithmetic fusion techniques have been proven successful in many cases, they have shortcomings. The additive fusion method tends to retain most of the clutter and background noise, whereas the multiplicative fusion method tends to suppress the targets with weak intensities. To address this problem, an image fusion method that maintains target intensities while suppressing clutter was proposed in [22], where the fuzzy logic approach was considered. Evaluation of the image fusion methods for TWRI has shown that the fuzzy logic approach outperforms the arithmetic fusion methods and produces an image with high target intensities and low clutter levels [22]. However, like most fuzzy logic-based fusion algorithms [12]–[14], [16], the method proposed in [22] requires manual selection of the fuzzy membership functions (MF) from the image intensity distributions. Since the distributions may vary between images, determining the optimal parameters for MF formulation becomes time-consuming.

In this paper, we propose a probabilistic fuzzy logic-based image fusion approach that overcomes the drawbacks of the

existing fuzzy logic methods. In the proposed approach, the fuzzy MFs are automatically selected, where the intensity distribution is modeled with a Gaussian-Rayleigh mixture. By appropriately modeling the image intensity distribution, the probability of a pixel value belonging to different regions can be determined, thereby automatically forming the respective MFs. Differing from the existing fuzzy logic method, the proposed approach does not require the fuzzification and defuzzification processes. Instead, the formulated membership values are used as weights in the fusion process, where a weighted sum of arithmetic operators is applied to the input images for fusion.

The existing arithmetic, DWT, PCA, fuzzy logic, and the proposed image fusion methods are evaluated and compared using real two-dimensional (2D) and three-dimensional (3D) polarimetric and multi-view images, collected at the Radar Imaging Lab, Center for Advanced Communications, Villanova University. The performance of the proposed approach in terms of enhancing target detection was also compared with the iterative likelihood ratio test (LRT) detector that fuses information obtained from multi-polarization and multi-view images at the decision level [23]. Experimental results show that the proposed probabilistic approach outperforms the existing image fusion methods, both qualitatively and quantitatively, by enhancing target regions and suppressing clutter. It is also observed that the proposed approach outperforms the LRT detector by producing an output image with a higher detection rate. Therefore, the proposed fusion approach can be used to enhance the performances of target detection methods [23], [24].

The remainder of this paper is organized as follows. Section II describes the existing pixel-level fuzzy logic-based fusion method for TWRI. Section III presents the proposed probabilistic fuzzy logic-based image fusion approach. Section IV analyzes the performance of the proposed approach on real 2D and 3D TWRI data, and Section V concludes the paper.

II. Existing Fuzzy Logic Approach

In this section, we discuss briefly the fuzzy logic approach for image fusion. Specifically, we consider the method introduced for pixel-level through-the-wall radar (TWR) image fusion that was proposed in [22]. The fuzzy logic approach is implemented through a Fuzzy Inference System (FIS) that formulates the mapping from two inputs to a single output. First, the inputs are converted into linguistic variables using a set of predefined MFs. In the fuzzification process, the degree of membership to a fuzzy set is determined for each input. Then, the inference engine is invoked, where fuzzy operators are applied to the fuzzified input images, based on a set of fuzzy rules. All the results are then aggregated and defuzzified to produce the final output. The flow chart of the FIS with two inputs and one output is shown in Fig. 1.

A. Fuzzy Membership Functions

The MFs are first formulated for the fuzzification process. As proposed in [22], a typical TWR image, with pixel values

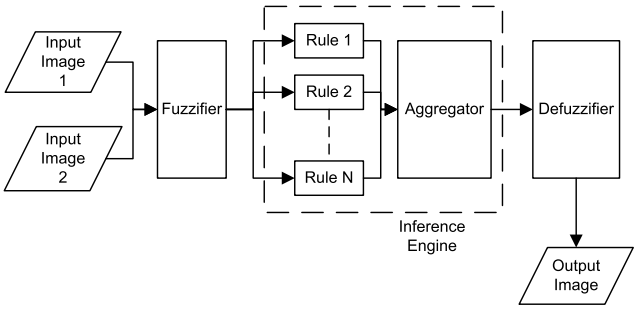

Fig. 1. Flow chart of a fuzzy inference system.

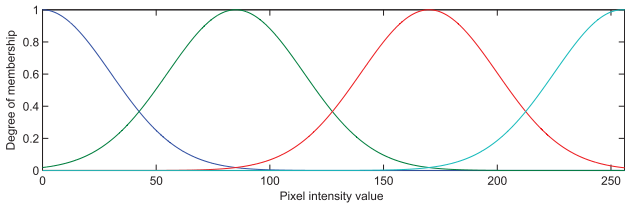

Fig. 2. An example of the formulated M membership functions, with $M = 4$, $\nu = \{0, 85, 170, 255\}$, $\sigma = 30$.

ranging from 0 to 255, can be divided into M regions, for instance, background noise, clutter, sidelobe, and targets. A simple method is to divide the intensity range into equal intervals. Each region is then formulated as a fuzzy set $\mathcal{F}_m$ $(m = 1, \ldots, M)$, represented with a Gaussian MF:

$$f_m(x; \sigma_m, c_m) = \exp\left\{-\frac{(x - c_m)^2}{2\sigma_m^2}\right\}, \tag{1}$$

where x is the intensity value, and σ_m and c_m are the width and the center of the MF. Figure 2 shows the MFs formulated in (1) for $M = 4$. Note that other segmentation techniques, such as K-means or fuzzy C-means clustering, can also be applied to determine the M regions.

After formulating the MFs, each pixel value x_i is assigned a value $\mu_m(x_i)$, which is its degree of membership to the fuzzy set $\mathcal{F}_m$. In other words, each crisp pixel value x_i is mapped to M membership degrees $\mu_m(x_i) = f_m(x_i)$, $m = 1, \ldots, M$. The value $\mu_m(x_1) = 1$ means that the intensity value x_i is fully a member of the m-th fuzzy set, whereas $0 < \mu_m(x_i) < 1$ indicates that x_i only partially belongs to the fuzzy set $\mathcal{F}_m$.

B. Fuzzy Rules

After fuzzifying the input images, fuzzy rules are then applied. Instead of using a global operator that is similar to pixel-wise addition or multiplication, operators in the form of IF-THEN statements are applied to the fuzzified images, based on a set of pre-determined rules. Consider two input images, X_1 and X_2, and the aim is to obtain the fused output image Y. Let x_1, x_2, and y denote the intensity values of a given pixel in X_1, X_2, and Y, respectively. The statement

$$(\text{IF } x_1 \text{ IS } \mathcal{F}_i) \text{ AND } (\text{IF } x_2 \text{ IS } \mathcal{F}_j) \text{ THEN } (y \text{ IS } \mathcal{G}_k),$$

can be represented as

$$R_q : \mathcal{F}_i \times \mathcal{F}_j \to \mathcal{G}_k, \quad i, j, k = 1, \ldots, M, \tag{2}$$

where R_q denotes the q-th fuzzy inference rule.

TABLE I
AN EXAMPLE OF FUZZY RULES FOR M FUZZY SETS AND N IMAGES, WHERE $M = 4$ AND $N = 2$

$\mathcal{F}_j$ \ $\mathcal{F}_i$	$\mathcal{F}_1$	$\mathcal{F}_2$	$\mathcal{F}_3$	$\mathcal{F}_4$
$\mathcal{F}_1$	$\mathcal{G}_1$	$\mathcal{G}_1$	$\mathcal{G}_3$	$\mathcal{G}_4$
$\mathcal{F}_2$	$\mathcal{G}_1$	$\mathcal{G}_2$	$\mathcal{G}_3$	$\mathcal{G}_4$
$\mathcal{F}_3$	$\mathcal{G}_3$	$\mathcal{G}_3$	$\mathcal{G}_3$	$\mathcal{G}_4$
$\mathcal{F}_4$	$\mathcal{G}_4$	$\mathcal{G}_4$	$\mathcal{G}_4$	$\mathcal{G}_4$

In fuzzy image fusion, the input and output fuzzy sets are defined on the same universe of discourse; therefore, albeit not necessary, the same MFs presented in (1) can be used to represent the output fuzzy sets, $\mathcal{G}_k,\ k = 1, \ldots, M$. Furthermore, in fuzzy fusion, the aim is to maintain or enhance certain regions (i.e., targets) and suppress others (i.e., clutter and background noise). To achieve this, we define the output fuzzy sets as follows:

$$\mathcal{G}_k = \begin{cases} \mathcal{G}_{\max\{i,j\}}, & \text{if } \max\{i, j\} > M/2, \\ \mathcal{G}_{\min\{i,j\}}, & \text{otherwise.} \end{cases} \tag{3}$$

For M membership functions and N input images, there are M^N fuzzy rules, denoted as R_q $(q = 1, \ldots, M^N)$. An example of the fuzzy rules for four fuzzy sets and two input images is summarized in Table I. The entry at column $\mathcal{F}_i$ and row $\mathcal{F}_j$ is the output fuzzy set $\mathcal{G}_k$.

For a given rule R_q, its firing strength (or weight) η_q is computed as a conjunction between the premise elements:

$$\eta_q = \mu_i(x_1) \wedge \mu_j(x_2), \quad q = (i-1)M + j, \tag{4}$$

where $\wedge$ denotes the conjunction operator. The minimum and product operators are the most commonly used conjunction operators; here, the minimum operator is used to compute the firing strength of each rule.

C. Aggregation and Defuzzification

Applying fuzzy operators to the input pixels produces a set of M^N rules R_q $(q = 1, \ldots, M^N)$. These rules are aggregated and then defuzzified using the centroid of area to convert the degree of membership and fuzzy set into a pixel value.

Here, the max-min operator is employed to compute the aggregate output MF. First, the qualified consequent MF for each rule is computed using the min operator $\hat{f}_q(x) = \min\{\eta_q, f_k(x)\}$, where $f_k(x)$ is the MF of the output fuzzy set G_k resulting from the rule R_q. Then, the overall output MF is obtained by aggregating the consequent MFs using the max operator:

$$f_A(x) = \max\{\hat{f}_1(x), \hat{f}_2(x), ..., \hat{f}_{M^N}(x)\}. \tag{5}$$

In other words, $f_A(x)$ is the aggregated MF curve produced by the union of all the consequent MFs. The defuzzification process is then applied to obtain the fused pixel value:

$$y = \frac{\int_{-\infty}^{\infty} f_A(x)x\ dx}{\int_{-\infty}^{\infty} f_A(x)\ dx}. \tag{6}$$

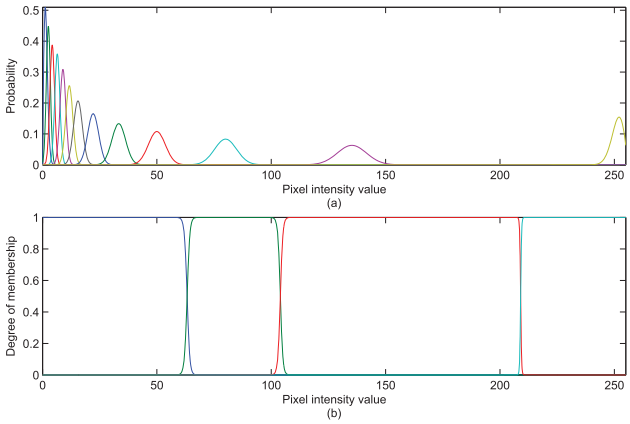

Fig. 3. An example of membership function formulation using the proposed approach: (a) K distributions from the Gaussian-Rayleigh mixture modeling, and (b) the formulated M membership functions, with $K = 13$ and $M = 4$.

Because the fuzzy logic-based fusion is a pixel-level operation, the fusion process is repeated for each pixel in the input images.

Albeit successful, the existing fuzzy logic approach requires manual formulation of the fuzzy MFs, which is generally obtained by observing the image intensity distributions. Since the acquired images depend on the imaging system, and the target location and orientation, determining the optimum fuzzy MFs can be time-consuming.

III. PROBABILISTIC FUZZY FUSION APPROACH

In this section, we present a new probabilistic approach for fuzzy logic-based image fusion to overcome the drawbacks of the existing fuzzy fusion methods. In the proposed approach, the fuzzy MFs are automatically learned, where the intensity distributions are modeled with a Gaussian-Rayleigh mixture. The degrees of membership to different regions are then used as weights in the fusion process, and a weighted sum of arithmetic operators is applied to the input images.

A. Automatic Formulation of Membership Functions

Unlike the fuzzy fusion method that requires manual selection of the fuzzy MFs, the proposed method uses an automated approach for MF formulation. It was shown in [23] that the probability density function (pdf) of TWR images generally resembles a combination of Gaussian and Rayleigh distributions. Thus, we propose to use a Gaussian-Rayleigh mixture to model the pdf of the observed TWR images. The number of mixture components K is automatically determined through the Bayesian information criterion (BIC) [25]. To reduce the number of rules, the K Gaussian-Rayleigh distributions are then combined to form M membership functions. Figure 3 shows an example of the automated MF formulation for $M = 4$ regions.

To date, automatic approaches for MF formulation, based on machine learning and statistical models, have been proposed to form trapezoidal and Gaussian MFs adaptively [26]–[30]. However, these methods were mostly proposed for a specific scenario, system, or dataset [31], [32]. In our approach, the MFs are learned from the pdf of the observed images using a mixture of Gaussian and Rayleigh distributions.

1) Gaussian-Rayleigh Mixture Modeling: In a typical TWR image, the lowest intensity values are mostly caused by clutter or background noise, whereas the highest intensity levels usually belong to the target regions. Because there is a high concentration of low pixel values and a low concentration of very high pixel values, the image intensity distribution tends to peak at both ends. Therefore, the noise and clutter region (with the lowest intensity levels) and the target regions (with the highest intensity levels) are more appropriately modeled as Rayleigh distributions

$$p_r(x) = \frac{x}{\sigma^2}\exp\left\{-\frac{x^2}{2\sigma^2}\right\}, \quad x \geq 0, \tag{7}$$

and the remaining regions are modeled as Gaussian distributions

$$p_g(x) = \frac{1}{\sqrt{2\pi\sigma^2}}\exp\left\{-\frac{(x-\nu)^2}{2\sigma^2}\right\}. \tag{8}$$

Similarly to the Gaussian mixture modeling-based segmentation [25], the Gaussian-Rayleigh mixture modeling uses the EM algorithm to estimate the mixture parameters. The proposed pdf can be expressed as a weighted sum of K class conditional pdfs:

$$p(x) = \sum_{k=1}^{K} \omega_k \ p_k(x|\boldsymbol{\theta}_k), \tag{9}$$

where ω_k is the component weight, and $\boldsymbol{\theta}_k$ represents the mixture parameters, $\boldsymbol{\theta}_k = (\nu_k, \sigma_k^2)$.

Let X denote the composite image formed by concatenating all input images, and let x_i $(i = 1, \ldots, Q)$ be the intensity value of the i-th pixel of X. Here, we assume the image X is lexicographically ordered into a $Q \times 1$ vector. The mixture parameters $\boldsymbol{\theta}_k$ $(k = 1, \ldots, K)$ are first estimated from the intensity distribution of the composite input image X. The conditional pdf of the k-th mixture component $p_k(x|\hat{\boldsymbol{\theta}}_k)$ is computed based on the current parameter estimate $\hat{\boldsymbol{\theta}}_k$,

$$p_k(x|\hat{\boldsymbol{\theta}}_k) = \begin{cases} \dfrac{x}{\hat{\sigma}_k^2}\exp\left\{-\dfrac{x^2}{2\hat{\sigma}_k^2}\right\} u(x), & \text{if } k = 1, \\ \dfrac{1}{\sqrt{2\pi\hat{\sigma}_k^2}}\exp\left\{-\dfrac{(x-\hat{\nu}_k)^2}{2\hat{\sigma}_k^2}\right\}, & \text{if } 1 < k < K, \\ \dfrac{255-x}{\hat{\sigma}_k^2}\exp\left\{-\dfrac{(255-x)^2}{2\hat{\sigma}_k^2}\right\} u(255-x), & \text{if } k = K, \end{cases} \tag{10}$$

where $u(x)$ is the unit step function. Once the conditional pdfs are computed, the posterior probability of class k, given pixel x_i, is determined as

$$\hat{P}_{k,i} = \frac{\hat{\omega}_k \ p_k(x_i|\hat{\boldsymbol{\theta}}_k)}{\sum_{k=1}^{K} \hat{\omega}_k \ p_k(x_i|\hat{\boldsymbol{\theta}}_k)}, \quad k = 1, \ldots, K. \tag{11}$$

Let Q be the total number of pixels in the composite image X. The component weights $\hat{\omega}_k$ and the parameter vector $\hat{\boldsymbol{\theta}}_k$ are then updated as

$$\hat{\omega}_k = \frac{1}{Q}\sum_{i=1}^{Q} \hat{P}_{k,i}, \tag{12}$$

$$\hat{\nu}_k = \begin{cases} 0, & \text{if } k = 1 \text{ or } K, \\ \dfrac{1}{Q}\displaystyle\sum_{i=1}^{Q} \frac{\hat{P}_{k,i} \ x_i}{\hat{\omega}_k}, & \text{if } 1 < k < K, \end{cases} \tag{13}$$

$$\hat{\sigma}_k^2 = \begin{cases} \dfrac{1}{Q}\displaystyle\sum_{i=1}^{Q} \frac{\hat{P}_{k,i} \ x_i^2}{\hat{\omega}_k}, & \text{if } k = 1 \text{ or } K, \\ \dfrac{1}{Q}\displaystyle\sum_{i=1}^{Q} \frac{\hat{P}_{k,i} \ (x_i - \hat{\nu}_k)^2}{\hat{\omega}_k}, & \text{if } 1 < k < K. \end{cases} \tag{14}$$

The steps of computing the conditional pdf, determining the posterior probability, and updating the component weights and parameter vector are repeated until the relative change in the the mixture parameter estimates is smaller than a tolerance $\varepsilon = 10^{-5}$.

In the Gaussian-Rayleigh mixture modeling method, the optimum number of mixture components K is determined by minimizing the BIC over K:

$$BIC = -2\sum_{i=1}^{Q} \log_{10}\left[p(x_i|K, \boldsymbol{\theta})\right] + K\log_{10}(Q), \tag{15}$$

where $p(x_i|K, \boldsymbol{\theta})$ is the conditional pdf in (9) for a given mixture model order K and the corresponding parameter vector $\boldsymbol{\theta}$.

2) Formation of Membership Functions: After obtaining the mixture parameter estimates, $\hat{\omega}_k$ and $\hat{\boldsymbol{\theta}}_k$ $(k = 1, \ldots, K)$, the K components in (10) are combined into M regions to form the MFs of the input fuzzy sets. Here, we define the M regions to be background noise, clutter/sidelobe, and two target regions (weak target and strong target regions). The clutter/sidelobe region overlaps with the weak target region on one side, and with the noise region on the other. Thus, we set the K-th component as the strong target region, the $(K-1)$-th component as the weak target region, and $(K-2)$-th component as the clutter/sidelobe region. The remaining $(K-3)$ components are combined to form the background noise region. The respective MFs for the M regions $(M = 4)$ are formed as

$$f_m(x) = \begin{cases} \displaystyle\sum_{k=1}^{K-3} \frac{\hat{\omega}_k \ p_k(x|\hat{\boldsymbol{\theta}}_k)}{p(x)}, & \text{if } m = 1, \\ \dfrac{\hat{\omega}_q \ p_q(x|\hat{\boldsymbol{\theta}}_q)}{p(x)}, \quad q = K-4+m, & \text{if } m = 2, 3, 4. \end{cases} \tag{16}$$

Figure 4 shows the segmented regions of an input image, which are determined by the proposed automated method for MF formulation. It can be observed that the proposed method successfully distinguishes between the target, clutter/sidelobe, and background noise regions.

The formulated MFs are then evaluated with the input pixel values. The output of each MF is a degree of membership $\mu_m(x_i)$ associated with the pixel value x_i. In other

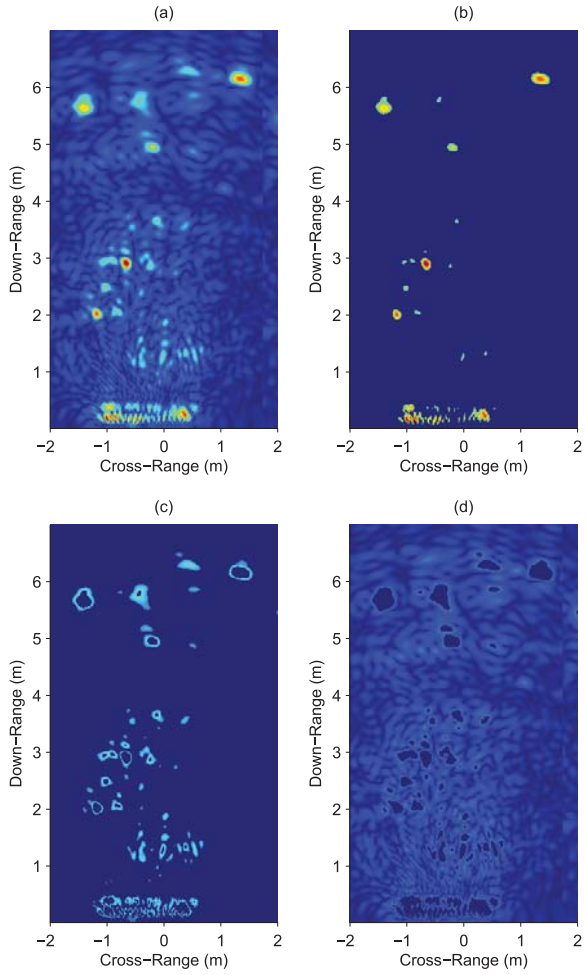

Fig. 4. An example of the segmented regions determined by the proposed approach: (a) input image, (b) strong and weak target region, (c) clutter/sidelobe region, and (d) background noise region.

words, (16) is evaluated by substituting the input pixel values to produce the set $\{\mu_1(x_i), \mu_2(x_i), \mu_3(x_i), \mu_4(x_i)\}$, where $\mu_m(x_i) \in [0, 1]$.

B. Fuzzy Fusion Operation

After determining the M degrees of membership of each pixel, we propose to use a combination of arithmetic operators, such as multiplication, maximum, and square root, for fusion. The fusion process is performed on the normalized input images. In the proposed approach, we apply the multiplicative operator to suppress the pixel values in the background noise and clutter/sidelobe regions. For the target regions, we apply the maximum operator to maintain all the pixel values in the weak target region, and the square root of the maximum to enhance the pixel values in the strong target region.

Consider N inputs images, $X_1, X_2, \ldots, X_N$. Let $x_{i,j}$ be the i-th pixel value of the j-th image. Here, we assume each image is transformed into a column vector using a lexicographical ordering. For each pixel $x_{i,j}$, we compute its degree of memberships $\mu_m(x_{i,j})$ $(m = 1, \ldots, 4)$ using (16). Let j^* denote the index of the largest pixel $x_{i,j}$ at the i-th position, for $j = 1, \ldots, N$; that is, $j^* = \arg\max_j \{x_{i,j}\}$. The output pixel value is calculated as a weighted sum of fused input regions:

$$y_i = \sum_{m=1}^{M} \mu_m(x_{i,j^*})\ F_m(x_{i,j}), \tag{17}$$

where the fused input region $F_m(x_{i,j})$ is given by

$$F_m(x_{i,j}) = \begin{cases} \prod_{j=1}^{N} x_{i,j}, & \text{if } m \le 2, \\ x_{i,j^*}, & \text{if } m = 3, \\ \sqrt{x_{i,j^*}}, & \text{if } m = 4. \end{cases} \tag{18}$$

The fusion process is repeated for each pixel in the input images.

IV. Experiments and Analysis

In this section, the proposed probabilistic fuzzy approach is evaluated on real 2D and 3D polarimetric images, collected at the Radar Imaging Lab, Center for Advanced Communications, Villanova University. The performance of the proposed approach is compared to the existing arithmetic and fuzzy fusion methods. Comparisons with the DWT and PCA image fusion methods that are commonly used in SAR imaging are also presented. In DWT fusion, the coefficients of the decomposed source images are fused prior to performing inverse DWT for image reconstruction. In PCA fusion, each pixel in the fused image is the weighted sum of the pixels in the input images, where the weights are the significant eigenvalues of the covariance matrix. In addition, the performance of the proposed approach in enhancing target detection, in terms of the detection rate, is also compared to an iterative LRT detection method proposed in [23]. In this article, the spatial units of all radar images are meters.

All images included in the following examples are generated based on frequency-domain backprojection [1]. We use an oversampled Cartesian grid for the range and cross-range variables. Note that high resolution imaging [33], [34] could be applied to the backprojection image before fusion, and using them as input images would lead to different results. In all cases, we assume that the reference empty scene is known, and is used for background subtraction, prior to image formation and fusion. Note also that wall clutter mitigation techniques [35], [36] can be employed in the case that background subtraction cannot be performed.

A. Experimental Setup

Two real scenes are considered in our experiments. The first scene consists of calibrated targets, acquired from a single viewpoint using multiple polarizations. The second scene is a populated scene with both calibrated targets and objects typically found in an office. The data corresponding to the populated scene are acquired from multiple views with a single polarization.

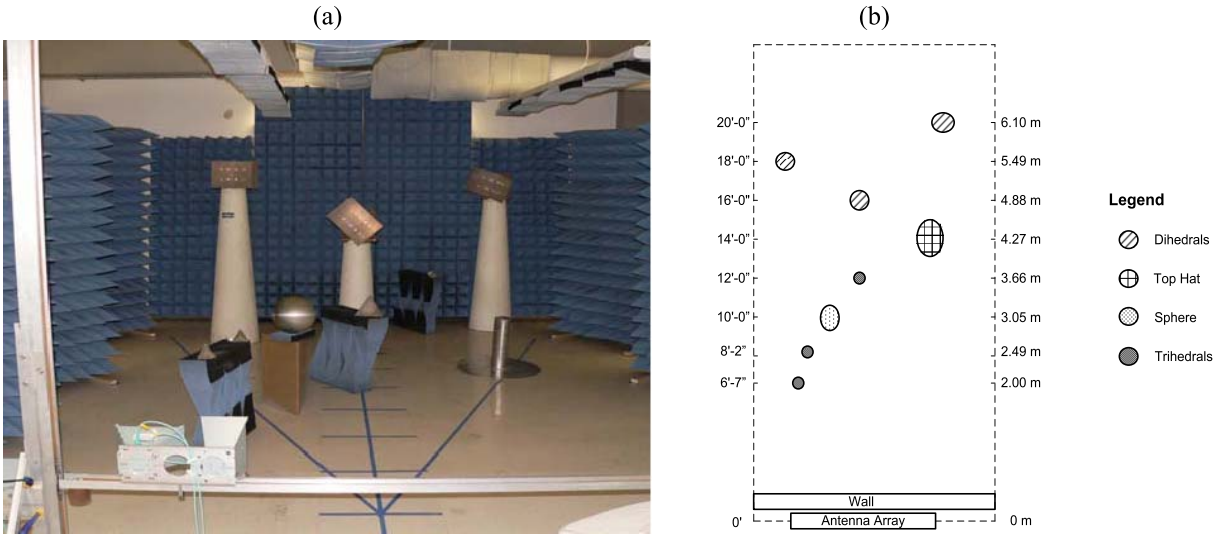

Fig. 5. The calibrated scene: (a) the scene is imaged through a non-homogenous plywood and gypsum wall; (b) the schematic diagram of the scene.

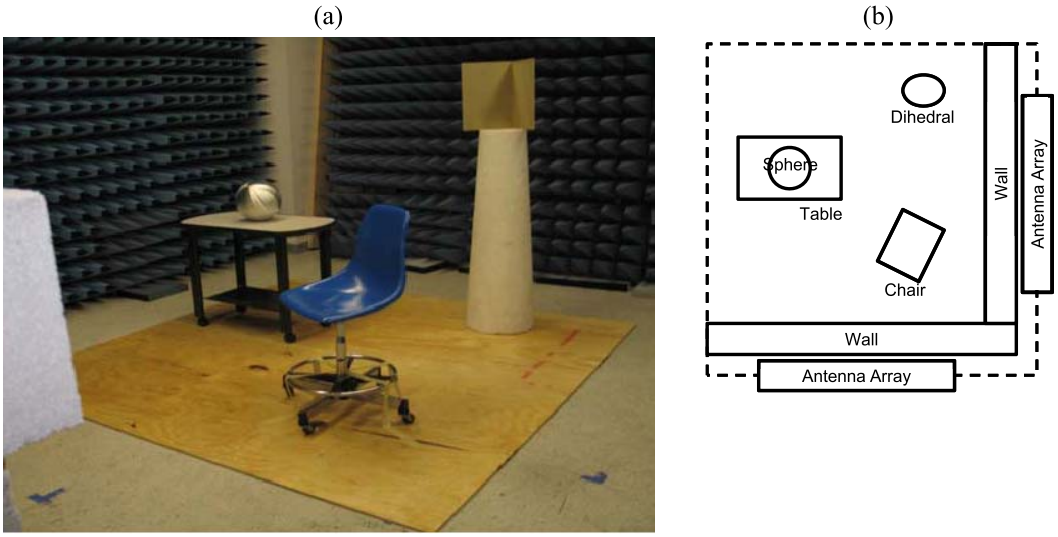

Fig. 6. The populated scene: (a) the scene is imaged through a homogenous concrete wall from two vantage points; (b) the schematic diagram of the scene.

1) Calibrated Scene: Horizontal and vertical polarization data sets are collected from a calibrated scene shown in Fig. 5. This scene contains a sphere, a top hat, a vertical dihedral, two dihedrals rotated at 22.5 and 45 degrees, and two trihedrals. These objects are placed at different downrange, cross-range and elevation bins. For each polarization setting, the scene is imaged with a 1 GHz stepped-frequency signal with a step size of 5 MHz and center frequency of 2.5 GHz. Imaging is performed through a non-homogenous plywood and gypsum board wall, using a 57-element linear array with an inter-element spacing of 22 mm. A total of 114 multiple polarization images are collected from the scene; each image has 214×161 pixels. Using the same physical hardware configuration, horizontal and vertical polarized 3D images are also acquired to produce images of size $214 \times 161 \times 57$ pixels.

2) Populated Scene: Multi-view vertical polarization data sets are also collected from a populated scene, which consists of a vertical dihedral, a sphere, a table with metal legs, and a chair. Each object is placed at different downrange, cross-range and height, as shown in Fig. 6. The data from the scene are collected using a stepped-frequency signal, consisting of 801 monochromatic frequencies with a 3 MHz step centered at 2.5 GHz, that is transmitted and received by a 57-by-57 element planar array with an inter-element spacing of 22 mm. Imaging is performed through a 140 mm thick homogeneous concrete wall from two vantage points, namely the front and the side views. Images of size 117×117 pixels, corresponding to the front and side views, at the heights of the dihedral and the table are acquired. The dihedral elevation represents an example of a scene with high signal-to-clutter ratio, whereas the images corresponding to the table elevation represent the case of low signal-to-clutter ratio.

B. Performance Measure

To evaluate the performance of the respective image fusion methods, the fused images are compared in terms of the

Improvement Factor in the Target-to-Clutter Ratio (IF) and the *target improvement factor* (TIF). The IF measures the overall enhancement of the output image, while the TIF measures the enhancement in the target regions only. Let $\mathcal{P}_{r,q}$ denote the average power of region r in image X_q, where r is a target or clutter region, and q is the input or output image. The IF is given by

$$\mathrm{IF} = 10\log_{10}\left[\frac{\mathcal{P}_{\mathrm{target,output}} \times \mathcal{P}_{\mathrm{clutter,input}}}{\mathcal{P}_{\mathrm{target,input}} \times \mathcal{P}_{\mathrm{clutter,output}}}\right], \tag{19}$$

and the TIF is defined as

$$\mathrm{TIF} = 10\log_{10}\left[\frac{\mathcal{P}_{\mathrm{target,output}}}{\mathcal{P}_{\mathrm{target,input}}}\right]. \tag{20}$$

The average power $\mathcal{P}_{r,q}$ can be expressed as

$$\mathcal{P}_{r,q} = \frac{1}{Q_r}\sum_{(k,l)\in r} X_q^2(k,l), \tag{21}$$

where Q_r is the number of pixels in region r. It should be noted that X_q in (19) and (20) consists of either the original images to be fused, or the fused image produced by the additive fusion. These images serve as a reference against which the improvement in image quality is assessed.

Albeit suitable as a contrast measure, a higher IF or TIF does not necessarily equal to better target detection. Hence, we also evaluate the performance of the image fusion methods in enhancing target detection. The receiver operation characteristics (ROC) curve is used to evaluate the probability of target detection. The probability of detection (PD), or detection rate, denotes the percentage of pixels in target regions that are correctly detected. Conversely, the probability of false alarm (PFA) or false alarm rate (FAR) is the percentage of pixels in non-target regions (background noise, clutter, and sidelobe) that are incorrectly detected. After normalizing the fused image, thresholds in an increment of 10^{-4} are applied to the image. At each threshold value, the respective ratios are calculated. For the calculations of the IF, TIF, PD and PFA, the pre-defined target and clutter regions for each scene (based on the ground truth) are provided in Figs. 7 to 9.

The detection rate obtained by applying simple thresholding to the fused images is also compared to that of an existing iterative LRT detection method [23]. Since the iterative LRT detection method requires a predefined FAR, the method is evaluated with a range of FAR values to obtain their respective PD values. The ROC curve produced by the iterative LRT detection method is then obtained.

During the detection process, the iterative LRT detector applies morphological filtering to obtain an improved detection result, where the size of the structuring element is automatically determined by the goodness-of-fit function [37]. Hence, we also apply a morphological filter, with the same type and size as that of the iterative LRT detector, as a post-processing step, to the output images produced by the fusion methods considered. The PD and PFA of the thresholded post-processed image are then calculated.

C. 2D Image Fusion

After image registration and normalization, the input images are fused using the proposed approach. The proposed approach is also compared with the additive, multiplicative, DWT, PCA and the existing fuzzy fusion method. Each method is applied to fuse multiple polarization images from the calibrated scene and multi-view images from the populated scene.

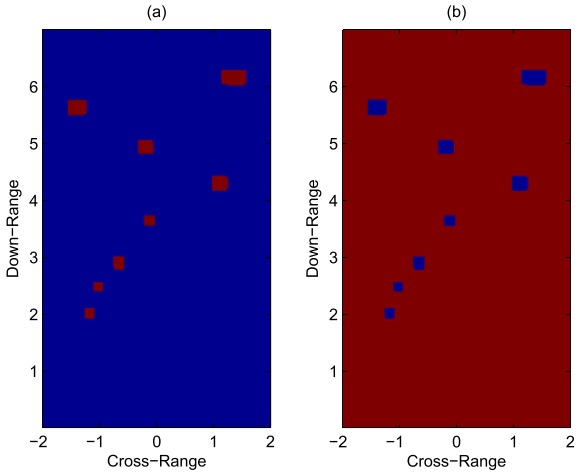

Fig. 7. The binary masks for the calibrated scene: (a) target mask; (b) clutter mask. See electronic color image.

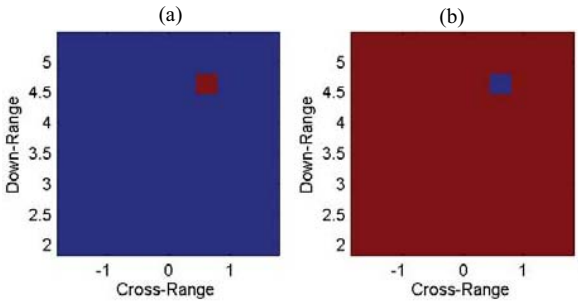

Fig. 8. The binary masks for the populated scene at the dihedral elevation: (a) target mask; (b) clutter mask. See electronic color image.

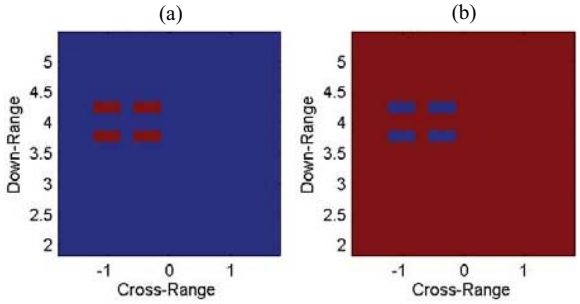

Fig. 9. The binary masks for the populated scene at the table elevation: (a) target mask; (b) clutter mask. See electronic color image.

1) Calibrated Scene: Figure 10 shows the input and output images, produced by the arithmetic, DWT, PCA and the fuzzy fusion methods, as well as the proposed probabilistic approach. By evaluating the image fusion methods on the 2D polarimetric imaging data, we observe that the additive fusion method (Fig. 10(c)) simply adds the images together and retains most of the background noise from both input images. This is evident from the IF (shown in Table II); the

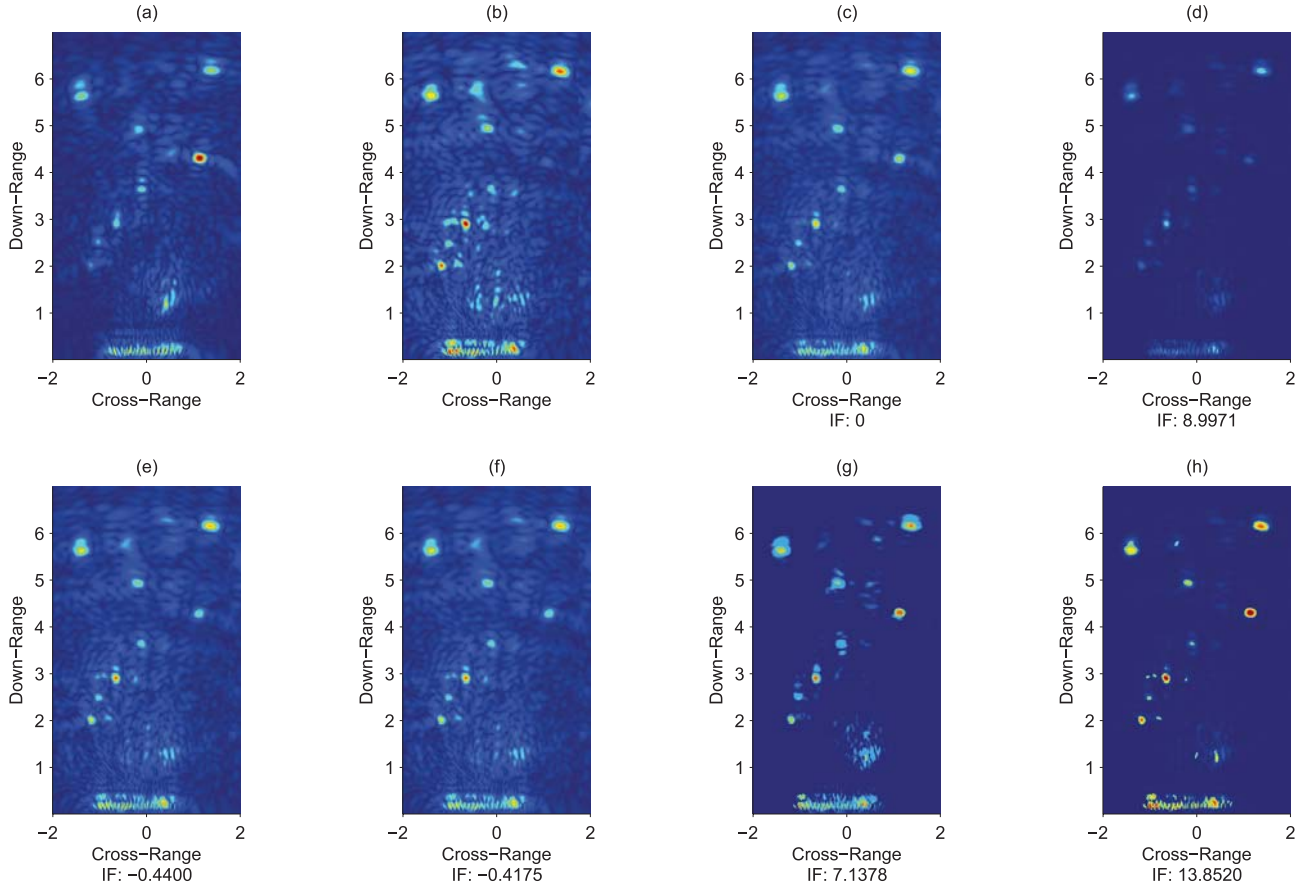

Fig. 10. Image fusion results of the calibrated scene: (a) horizontal and (b) vertical polarization input images, and output images from the (c) additive, (d) multiplicative, (e) DWT, (f) PCA, and the (g) existing and (h) proposed fuzzy logic-based image fusion methods.

additive fusion method produces a degraded image when using the horizontal polarization image as a reference. This is due to the maintenance of the background noise and clutter from the vertical polarization image. Similarly, both DWT and PCA fusion methods also retain most of the noise, as shown in Figs. 10(e) and 10(f), and produce degraded images that are poorer than that of the additive fusion. The multiplicative fusion method (Fig. 10(d)) reduces the background noise, but it also reduces the target intensities. This reduction is caused by the enhancement of overlapping pixels in both input images, while non-overlapping pixels are suppressed through multiplication. While both fuzzy logic-based fusion methods successfully maintain all the targets and suppress clutter, the proposed probabilistic approach produces an output image with the highest IF, as shown in Table II.

When we consider target regions only, Table III shows that all the methods evaluated outperform the multiplicative fusion. This is because multiplicative fusion suppresses the intensity levels of the targets. Among all the methods tested, the proposed probabilistic approach produces an output image with the highest TIF.

Each fused image is then normalized and thresholded to calculate the PD and PFA. Figure 11 shows the ROC curves produced by applying simple thresholding to the output of the proposed probabilistic fuzzy fusion approach and the input images. It is observed that by fusing the input images, the proposed approach improves target detection. Figure 12 shows the ROC curves produced by thresholding the output images of all the fusion methods considered, as well as that of the iterative LRT detector. We observe that the proposed approach

TABLE II
IMPROVEMENT FACTOR IN THE TARGET-TO-CLUTTER RATIOS (IF) IN dB OF THE DIFFERENT IMAGE FUSION METHODS FOR THE CALIBRATED SCENE

Method	*Horizontal Polarization*	*Vertical Polarization*	*Additive Fusion*
Additive fusion	-1.6687	1.3262	0
Multiplicative fusion	7.3283	10.3233	8.9971
DWT fusion	-2.1087	0.8862	-0.4400
PCA fusion	-2.0862	0.9087	-0.4175
Fuzzy fusion	5.4690	8.4640	7.1378
Probabilistic fuzzy fusion	**12.1833**	**15.1782**	**13.8520**

TABLE III
TARGET IMPROVEMENT FACTOR (TIF) IN dB OF THE DIFFERENT IMAGE FUSION METHODS FOR THE CALIBRATED SCENE

Method	*Horizontal Polarization*	*Vertical Polarization*	*Additive Fusion*
Additive fusion	0.3095	-1.2465	0
Multiplicative fusion	-7.5777	-9.1338	-7.8872
DWT fusion	0.5841	-0.9719	0.2747
PCA fusion	0.5684	-0.9876	0.2589
Fuzzy fusion	0.6028	-0.9532	0.2933
Probabilistic fuzzy fusion	**1.6999**	**0.1439**	**1.3904**

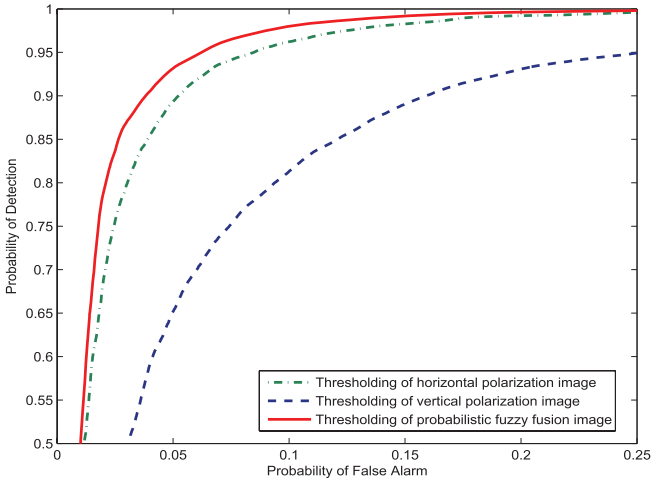

Fig. 11. Receiver operating characteristics curves of the thresholding of input images and the proposed probabilistic fuzzy fusion approach.

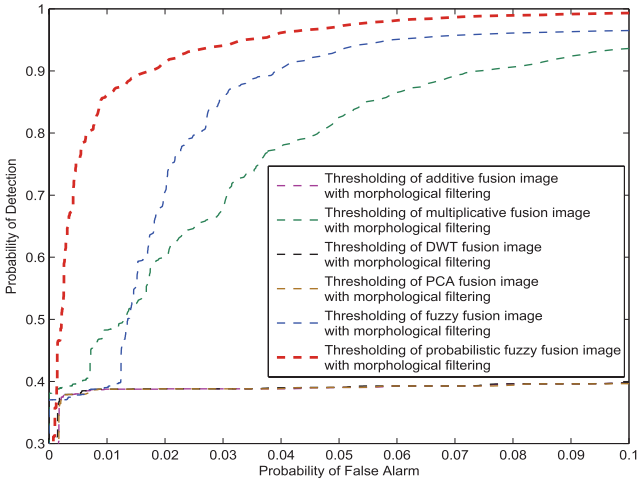

Fig. 13. Receiver operating characteristics curves of the thresholding of all the image fusion methods with morphological filtering. See electronic color image.

TABLE IV
PROBABILITY OF DETECTION AT 5% FALSE ALARM RATE

Method	*Detection Rate (%)*
Thresholding of additive fusion image	92.87
Thresholding of multiplicative fusion image	91.23
Thresholding of DWT fusion image	89.91
Thresholding of PCA fusion image	90.37
Thresholding of fuzzy fusion image	91.21
Thresholding of probabilistic fuzzy fusion image	93.16
Thresholding of probabilistic fuzzy fusion image with morphological filtering	**97.13**
Iterative LRT detector	92.77

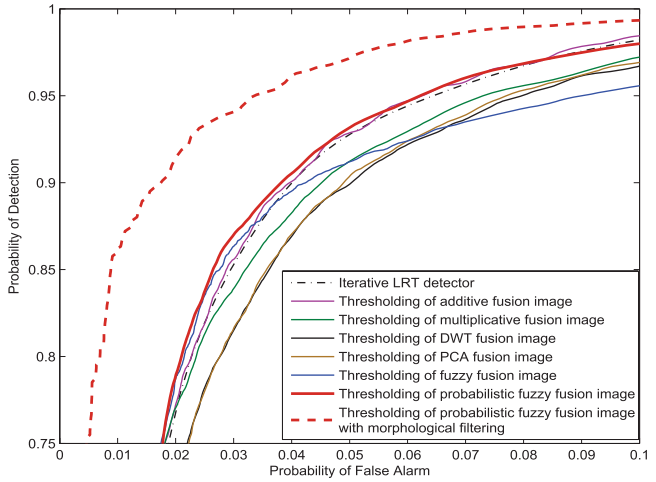

Fig. 12. Receiver operating characteristics curves of the iterative LRT detector and the thresholding of the five image fusion methods and the proposed approach with and without morphological filtering. See electronic color image.

leads to higher PD rate, compared to the other five fusion methods and the LRT detector. Applying the morphological filter as a post-processing step further improves the detection rate of the proposed approach. When applying the morphological filter to the outputs of the other fusion methods, we observe from Fig. 13 that the filtered image produced by the proposed approach has a higher detection rate. While the morphological filter enhances the performance of the fuzzy logic approaches, it reduces the performance of the other fusion methods. Table IV shows the PD at 5% FAR for the iterative LRT detector and the thresholding of images produced by the five fusion methods and the proposed approach with and without post-processing. Note that because the morphological filter did not improve the performance of the non-fuzzy fusion methods (see Fig. 13), the detection rates calculated are not included in Table IV.

With a high IF, TIF and the ability to enhance target detection, the proposed approach is proven effective for pixel-level TWR image fusion.

2) Populated Scene: Figure 14 shows the registered input and output images centered at the dihedral elevation, along with the fusion results from the arithmetic, DWT, PCA, and the fuzzy fusion methods. As shown in Figs. 14(c), 14(e) and 14(f), the additive, DWT and PCA image fusion methods retain most of the background noise. Although the multiplicative fusion method (Fig. 14(d)) reduces the background noise, it also reduces the target region. In comparison, both fuzzy logic-based fusion methods maintain the targets, while suppressing clutter. It can be observed from Fig. 14 that the proposed probabilistic approach produces an output image that has less clutter than the fuzzy fusion method. The output image also has the highest IF, as presented in Table V.

Similar to the results of the calibrated scene, Table VI shows that the multiplicative fusion method generally has a negative TIF. This is due to its over-suppression and reduction of the target regions. Since the fuzzy fusion method retains the target with the highest intensity levels, the TIF produced is also the highest among all the methods considered. The proposed probabilistic approach also maintains targets to produce a similar result to that of the fuzzy fusion. Since the additive fusion maintains most of the clutter, and both the DWT and PCA fusion methods are unable to maintain the full shape of

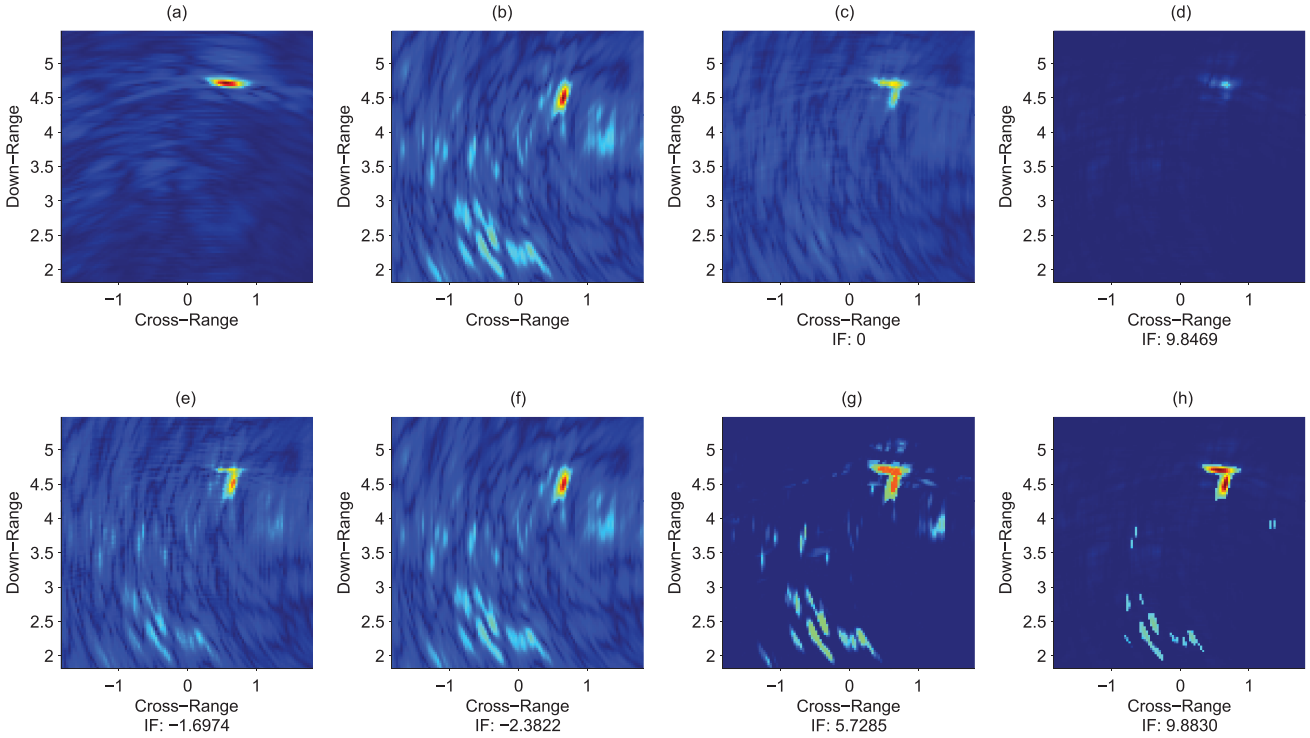

Fig. 14. Image fusion results of the populated scene (dihedral level): (a) front and (b) side views of the dihedral elevation, and output images from the (c) additive, (d) multiplicative, (e) DWT, (f) PCA, and the (g) existing and (h) proposed fuzzy logic-based image fusion methods.

TABLE V

IMPROVEMENT FACTOR IN THE TARGET-TO-CLUTTER RATIOS (IF) IN dB OF THE DIFFERENT IMAGE FUSION METHODS FOR THE POPULATED SCENE (AT DIHEDRAL LEVEL)

Method	*Front View*	*Side View*	*Additive Fusion*
Additive fusion	-6.4902	2.5040	0
Multiplicative fusion	3.3567	12.3509	9.8469
DWT fusion	-8.1877	0.8066	-1.6974
PCA fusion	-8.8724	0.1219	-2.3822
Fuzzy fusion	-0.7617	8.2326	5.7285
Probabilistic fuzzy fusion	**3.3928**	**12.3870**	**9.8830**

TABLE VI

TARGET IMPROVEMENT FACTOR (TIF) IN dB OF THE DIFFERENT IMAGE FUSION METHODS FOR THE POPULATED SCENE (AT DIHEDRAL LEVEL)

Method	*Front View*	*Side View*	*Additive Fusion*
Additive fusion	-0.8472	-1.6330	0
Multiplicative fusion	-11.1122	-11.8980	-10.2650
DWT fusion	-0.0950	-0.8808	0.7523
PCA fusion	0.5372	-0.2486	1.3844
Fuzzy fusion	**2.2966**	**1.5108**	**3.1438**
Probabilistic fuzzy fusion	2.1694	1.3836	3.0166

the target, all three methods produce a TIF that is lower than that of the probabilistic fuzzy fusion approach.

In Fig. 15, the registered input images obtained at the table elevation are shown together with the respective outputs obtained from the six image fusion methods. Figures 15(a) and 15(b) clearly show the metal legs of the table at the correct locations (depicted as white circles). However, due to the low signal-to-noise ratio, it is difficult to discern the targets' presence without any prior knowledge. Through image fusion, all the image fusion methods did not perform well enough to distinguish the target's presence. This is because there is heavy clutter with similar or higher intensity values than the target pixels. Although the multiplicative fusion has the highest IF, as shown in Table VII, we observe that both target and clutter were suppressed. The fuzzy logic-based methods, on the other hand, retain most of the targets. However, due to the high clutter pixel values, the fuzzy logic approaches also retained them in the fused results, thus producing an output image with low IF. It is generally observed that the proposed approach produces images with high IF, except when the input images have low signal-to-clutter ratio.

TABLE VII

IMPROVEMENT FACTOR IN THE TARGET-TO-CLUTTER RATIOS (IF) IN dB OF THE DIFFERENT IMAGE FUSION METHODS FOR THE POPULATED SCENE (AT TABLE LEVEL)

Method	*Front View*	*Side View*	*Additive Fusion*
Additive fusion	-0.3039	0.9911	0
Multiplicative fusion	**4.6467**	**5.9417**	**4.9506**
DWT fusion	-0.3511	0.9438	-0.0472
PCA fusion	-0.3032	0.9917	0.0006
Fuzzy fusion	0.5837	1.8786	0.8876
Probabilistic fuzzy fusion	2.5932	3.8881	2.8971

Table VIII presents the target enhancements results for all the fusion methods considered. The results in this table show that the multiplicative fusion generates an output image with the lowest TIF, due to the suppression of targets. In contrast, the proposed approach produces an output image with high target and low clutter levels, and therefore has a higher TIF compared to the other methods considered.

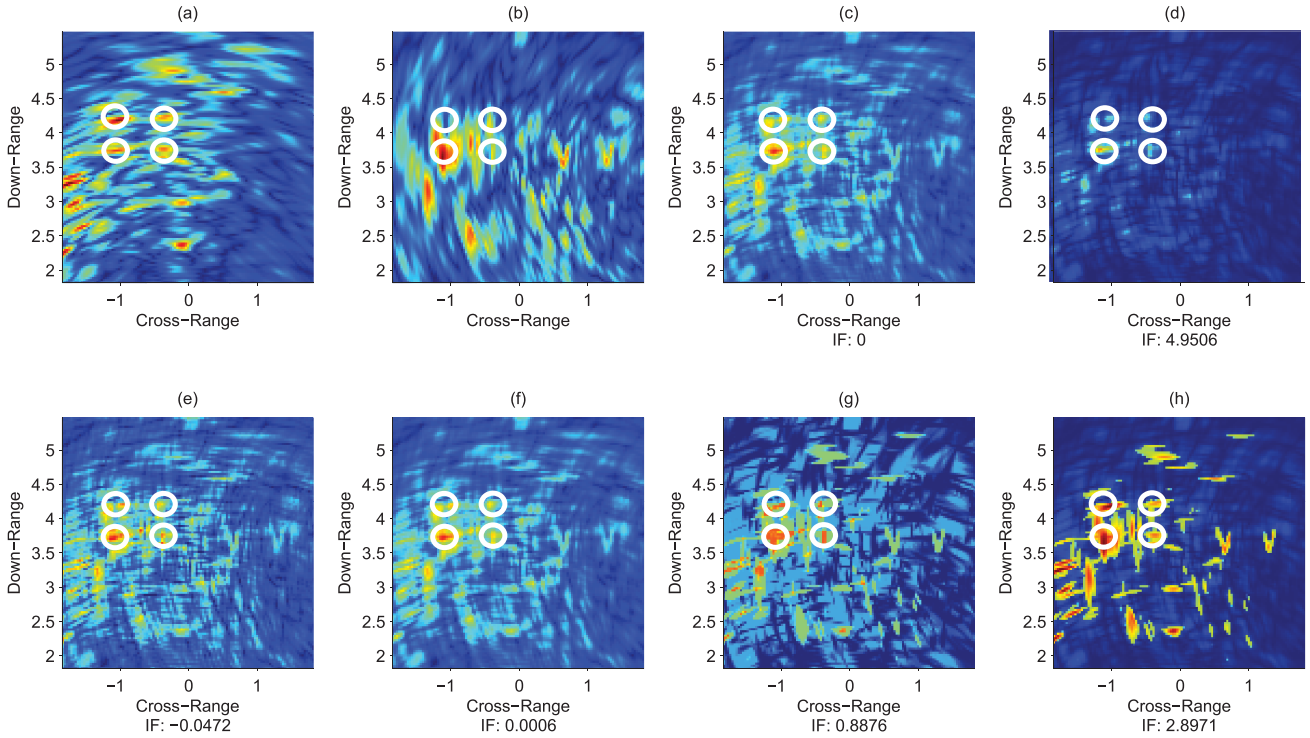

Fig. 15. Image fusion results of the populated scene (table level): (a) front and (b) side views of the table elevation, and output images from the (c) additive, (d) multiplicative, (e) DWT, (f) PCA, and the (g) existing and (h) proposed fuzzy logic-based image fusion methods.

TABLE VIII
TARGET IMPROVEMENT FACTOR (TIF) IN dB OF THE DIFFERENT IMAGE FUSION METHODS FOR THE POPULATED SCENE (AT TABLE LEVEL)

Method	*Front View*	*Side View*	*Additive Fusion*
Additive fusion	-0.8862	0.3403	0
Multiplicative fusion	-6.0073	-4.7808	-5.1210
DWT fusion	-0.7939	0.4326	0.0923
PCA fusion	-0.8856	0.3409	0.0006
Fuzzy fusion	-0.2319	0.9946	0.6543
Probabilistic fuzzy fusion	**0.3700**	**1.5965**	**1.2562**

TABLE IX
PROBABILITY OF DETECTION AT 5% FALSE ALARM RATE

Scene	*Method*	*Detection Rate (%)*
Dihedral level	Thresholding of additive fusion image	57.39
	Thresholding of multiplicative fusion image	67.33
	Thresholding of DWT fusion image	40.39
	Thresholding of PCA fusion image	30.19
	Thresholding of fuzzy fusion image	55.48
	Thresholding of probabilistic fuzzy fusion image	67.57
	Thresholding of probabilistic fuzzy fusion image with morphological filtering	**71.75**
	Iterative LRT detector	40.78
Table level	Thresholding of additive fusion image	58.43
	Thresholding of multiplicative fusion image	58.19
	Thresholding of DWT fusion image	54.20
	Thresholding of PCA fusion image	58.47
	Thresholding of fuzzy fusion image	49.01
	Thresholding of probabilistic fuzzy fusion image	53.82
	Thresholding of probabilistic fuzzy fusion image with morphological filtering	**61.97**
	Iterative LRT Detector	58.26

We also apply thresholding to the normalized fused images to calculate the PD and PFA. Table IX shows the detection rate at 5% FAR for all the fusion methods, as well as for the proposed approach with morphological filtering. The detection rates are also compared to that obtained by the iterative LRT detector. It can be observed that the proposed probabilistic fuzzy fusion approach generally has the highest detection rate, except when the clutter has a similar or higher intensity value than the target pixels. In the low signal-to-clutter ratio scenario, the iterative LRT detector produces a higher detection rate than the proposed approach; however, LRT detection rate is still lower than the other image fusion methods considered. After applying the morphological filter, the proposed approach outperforms the iterative LRT detector by producing an output image with a higher detection rate.

The experimental results indicate that the additive, DWT and PCA fusion methods maintain most of the background noise and clutter. In some cases, the target pixel values are also reduced. This is because the three methods use addition as a fusion operator, which is similar to the averaging operator. Thus, some targets are enhanced, while others are suppressed during fusion. As a result, the produced image has a poor IF, albeit having a high PD. The experimental results also indicate that the multiplicative fusion produces an output image with a high IF. However, this is only valid when target pixels are located at the same location in the input images. Otherwise, all the pixel values will be suppressed, and an output image with low TIF will be produced. Due to the over-suppression

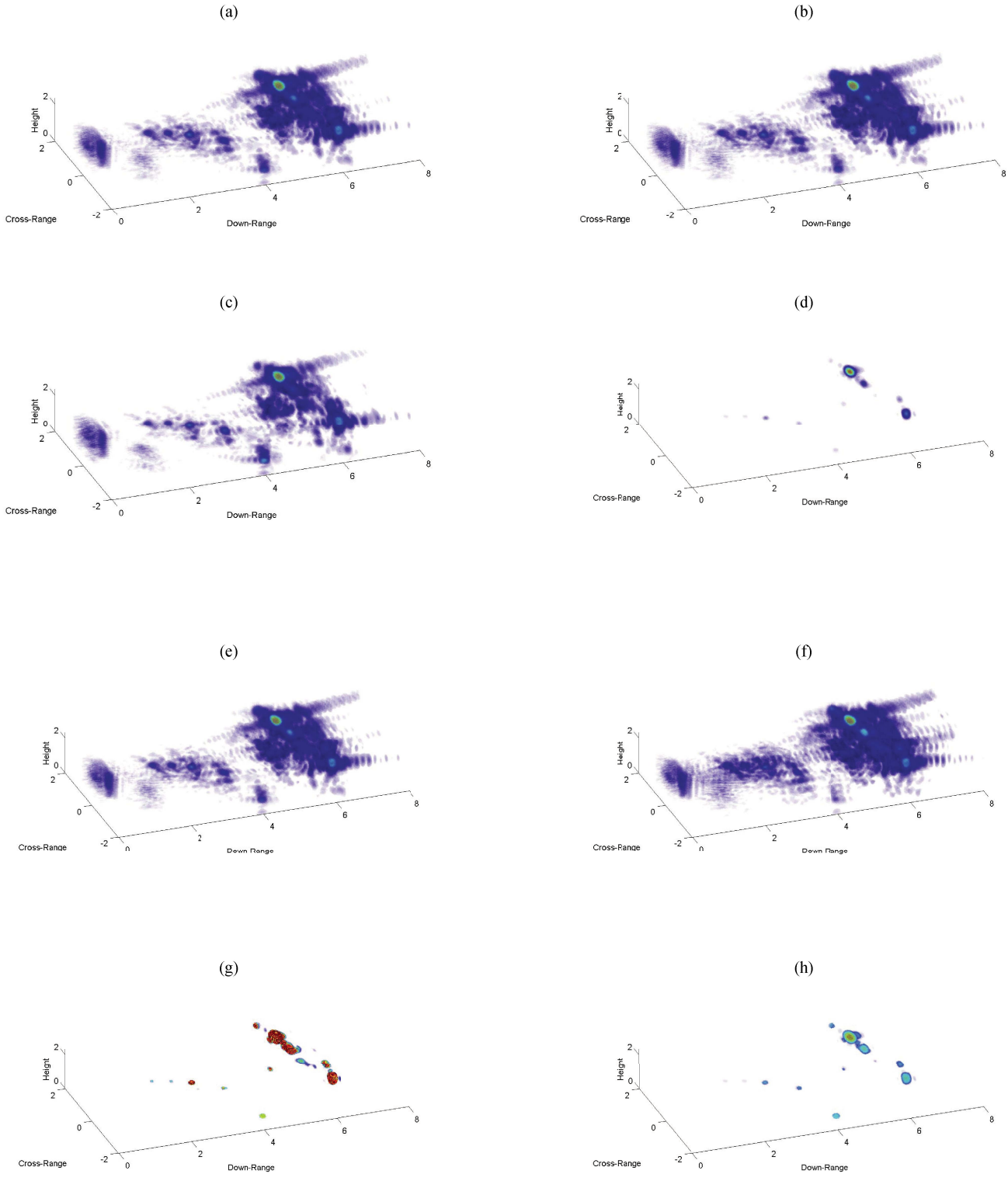

Fig. 16. Three dimensional image fusion results: (a) horizontal and (b) vertical polarization input images, and output images from the (c) additive, (d) multiplicative, (e) DWT, (f) PCA, and the (g) existing and (h) proposed fuzzy logic-based image fusion methods.

of the pixel values, the multiplicative fusion does not enhance target detection significantly.

In comparison, the proposed approach produces a fusion result with a high IF, and enhances target detection. This is evident when clutter pixel values in the input images are lower than that of the target pixels. Because targets generally have high pixel values, when the input images have low signal-to-clutter ratios, the proposed approach may not perform well. However, this reduction in performance for scenes with low signal-to-clutter ratio applies to not only the

proposed approach but also to all other methods evaluated. To improve the performance of the proposed approach, morphological filtering can be applied as a post-processing step after fusion. Alternatively, image enhancement techniques, such as image restoration or image segmentation, can be applied to the input images, prior to fusion.

D. 3D Image Fusion

Using the polarimetric 3D images collected from the calibrated scene, we compare the performances of the additive, multiplicative, DWT, PCA and the fuzzy logic-based fusion methods. Figure 16 shows the input and output images, produced by the additive, multiplicative, DWT, PCA, fuzzy and the proposed probabilistic fuzzy fusion methods. Similar to the results on 2D image fusion, the additive, DWT and PCA fusion retain most of the noise from both input images. Although the multiplicative fusion manages to suppress the noise, targets intensities are also reduced. The fuzzy logic approaches produce a balanced output image that has low clutter and high target intensities. Furthermore, the proposed approach produces images with less clutter compared to the existing fuzzy fusion method.

V. Conclusion

In this paper, we have proposed a probabilistic approach to fuzzy logic-based image fusion. The proposed approach applies the Gaussian-Rayleigh mixture modeling to automatically formulate the MFs, which are then employed for image fusion in through-the-wall radar imaging. Experimental results based on real 2D and 3D polarimetric and multi-view data demonstrate the effectiveness of the proposed approach for pixel-level image fusion. The proposed fuzzy logic-based image fusion approach, which is free from human intervention, was compared with several existing fusion methods for TWR images and was shown to improve both image contrast and target detection.

References

[1] M. Amin, *Through the Wall Radar Imaging*. Boca Raton, FL, USA: CRC Press, 2010.

[2] M. Amin and F. Ahmad, "Wideband synthetic aperture beamforming for through-the-wall imaging," *IEEE Signal Process. Mag.*, vol. 25, no. 4, pp. 110–113, Jul. 2008.

[3] D. D. Ferris, and N. C. Currie, "A survey of current technologies for through-the-wall surveillance (TWS)," *Proc. SPIE*, vol. 3577, pp. 62–72, Jan. 1999.

[4] A. Gaugue and J. Politano, "Overview of current technologies for through-the-wall-surveillance," *Proc. SPIE* vol. 5989, pp. 1–11, Nov. 2005.

[5] H. Griffiths and C. Baker, "Radar imaging for combatting terrorism," in *Imaging for Detection and Identification*. New York, NY, USA: Springer-Verlag, 2006.

[6] Y. Zhang and M. Amin, "Joint Doppler and polarization characterization of moving targets," in *Proc. IEEE Antennas Propag. Soc. Conf.*, Jun. 2004, pp. 3083–3086.

[7] S. Hong, W. Moon, H. Paik, and G. Choi, "Data fusion of multiple polarimetric SAR images using discrete wavelet transform (DWT)," in *Proc. IEEE IGARSS*, vol. 6. Jun. 2002, pp. 3323–3325.

[8] L. Fonseca, L. Namikawa, and E. Castejon, "Digital image processing in remote sensing," in *Proc. 22nd Brazilian Symp. Comput. Graph. Image Process.*, 2009, pp. 59–71.

[9] M. Nakamura, Y. Yamaguchi, and H. Yamada, "Real-time and full polarimetric FM-CW radar and its application to the classification of targets," *IEEE Trans. Instrum. Meas.*, vol. 47, no. 2, pp. 572–577, Apr. 1998.

[10] A. Nashashibi, K. Sarabandi, P. Frantzis, R. De Roo, and F. Ulaby, "An ultrafast wide-band millimeter-wave (MMW) polarimetric radar for remote sensing applications," *IEEE Trans. Geosci. Remote Sens.*, vol. 40, no. 8, pp. 1777–2002, Aug. 2002.

[11] D. Sheen, D. McMakin, and T. Hall, "Near field imaging at microwave and millimeter wave frequencies," in *Proc. IEEE Int. Microw. Symp.*, Jun. 2007, pp. 1693–1696.

[12] T. Meitzler, D. Bryk, E. Sohn, K. Lane, J. Raj, and H. Singh, "Fuzzy logic based sensor fusion for mine and concealed weapon detection," *Proc. SPIE*, vol. 5089, pp. 1353–1362, Sep. 2003.

[13] Z. Mengyu and Y. Yuliang, "A new image fusion algorithm based on fuzzy logic," in *Proc. ICICTA*, Oct. 2008, pp. 83–86.

[14] J. Saeedi and K. Faez, "The new segmentation and fuzzy logic based multi-sensor image fusion," in *Proc. IVCNZ*, Nov. 2009, pp. 328–333.

[15] P. Gamba, F. Dell'Acqua, and B. Dasarathy, "Urban remote sensing using multiple data sets: Past, present, and future," *Inf. Fusion*, vol. 6, no. 4, pp. 319–326, Dec. 2005.

[16] A. Filippidis, L. Jain, and N. Martin, "Fuzzy rule based fusion technique to automatically detect aircraft in SAR images," in *Proc. 1st Int. Conf. KES*, vol. 2. May 1997, pp. 435–441.

[17] C. Pohl and J. Van Genderen, "Multisensor image fusion in remote sensing: Concepts, methods and applications," *Int. J. Remote Sens.*, vol. 19, no. 5, pp. 823–854, 1998.

[18] F. Ahmad and M. Amin, "Multi-location wideband synthetic aperture imaging for urban sensing applications," *J. Franklin Inst.*, vol. 345, no. 6, pp. 618–639, Sep. 2008.

[19] G. Wang and M. Amin, "Imaging through unknown walls using different standoff distances," *IEEE Trans. Signal Process.*, vol. 54, no. 10, pp. 4015–4025, Oct. 2006.

[20] F. Ahmad and M. Amin, "Through-the-wall polarimetric imaging," *Proc. SPIE*, vol. 6970, pp. 1–10, Apr. 2008.

[21] T. Dogaru and C. Le, "SAR images of rooms and buildings based on FDTD computer models," *IEEE Trans. Geosci. Remote Sens.*, vol. 47, no. 5, pp. 1388–1401, May 2009.

[22] C. Seng, A. Bouzerdoum, F. Tivive, and M. Amin, "Fuzzy logic-based image fusion for multi-view through-the-wall radar," in *Proc. Int. Conf. DICTA*, Dec. 2010, pp. 423–428.

[23] C. Debes, M. Amin, and A. Zoubir, "Target detection in single-and multiple-view through-the-wall radar imaging," *IEEE Trans. Geosci. Remote Sens.*, vol. 47, no. 5, pp. 1349–1361, May 2009.

[24] S. Papson and R. Narayanan, "Multiple location SAR/ISAR image fusion for enhanced characterization of targets," *Proc. SPIE*, vol. 5788, pp. 128–139, Aug. 2005.

[25] O. Demirkaya, M. Asyali, and P. Sahoo, *Image Processing with MATLAB Applications in Medicine and Biology*. Boca Raton, FL, USA: CRC Press, 2008.

[26] A. Homaifar and E. McCormick, "Simultaneous design of membership functions and rule sets for fuzzy controllers using genetic algorithms," *IEEE Trans. Fuzzy Syst.*, vol. 3, no. 2, pp. 129–139, May 1995.

[27] G. Liu and W. Yang, "Learning and tuning of fuzzy membership functions by simulated annealing algorithm," in *Proc. IEEE APCCAS*, Dec. 2000, pp. 367–370.

[28] M. Makrehchi, O. Basir, and M. Kamel, *Generation of Fuzzy Membership Function Using Information Theory Measures and Genetic Algorithm*. Berlin, Germany: Springer-Verlag, 2003, pp. 603–610.

[29] I. Derbel, N. Hachani, and H. Ounelli, "Membership functions generation based on density function," in *Proc. Int. Conf. CIS*, vol. 1. Dec. 2008, pp. 96–101.

[30] R. Hosseini, S. Qanadli, S. Barman, M. Mazinani, T. Ellis, and J. Dehmeshki, "An automatic approach for learning and tuning gaussian interval type-2 fuzzy membership functions applied to lung CAD classification system," *IEEE Trans. Fuzzy Syst.*, vol. 20, no. 2, pp. 224–234, Aug. 2012.

[31] J. Bezdek, "Fuzzy models—What are they, and why?" *IEEE Trans. Fuzzy Syst.*, vol. 1, no. 1, pp. 1–6, Feb. 1993.

[32] B. Bouchon-Meunier, M. Dotoli, and B. Maione, "On the choice of membership functions in a mandani-type fuzzy controller," in *Proc. 1st Online Workshop Soft Comput.*, 1996, pp. 1–6.

[33] Y.-S. Yoon and M. Amin, "High-resolution through-the-wall radar imaging using beamspace MUSIC," *IEEE Trans. Antennas Propag.*, vol. 56, no. 6, pp. 1763–1774, Jun. 2008.

[34] Y.-S. Yoon, M. Amin, and F. Ahmad, "MVDR beamforming for through-the-wall radar imaging," *IEEE Trans. Aerosp. Electron. Syst.*, vol. 47, no. 1, pp. 347–366, Jan. 2011.
[35] Y.-S. Yoon and M. Amin, "Spatial filtering for wall-clutter mitigation in through-the-wall radar imaging," *IEEE Trans. Geosci. Remote Sens.*, vol. 47, no. 9, pp. 3192–3208, Sep. 2009.
[36] F. Tivive, A. Bouzerdoum, and M. Amin, "An SVD-based approach for mitigating wall reflections in through-the-wall radar imaging," in *Proc. IEEE Radar Conf.*, May 2011, pp. 519–524.
[37] C. Debes, J. Riedler, A. Zoubir, and M. Amin, "Adaptive target detection with application to through-the-wall radar imaging," *IEEE Trans. Signal Process.*, vol. 58, no. 11, pp. 5572–5583, Nov. 2010.

Cher Hau Seng received the B.E. (Hons.) degree in computer engineering from the University of Wollongong, Wollongong, Australia. He is currently pursuing the Ph.D. degree with the School of Electrical, Computer and Telecommunications Engineering, University of Wollongong. His general research interests include the area of image processing with applications to radar and medical imaging.

Abdesselam Bouzerdoum (M'89–SM'03) is the Professor of computer engineering and an Associate Dean (Research) with the Faculty of Informatics, University of Wollongong, Wollongong, Australia. He received the M.Sc. and Ph.D. degrees from the University of Washington, Seattle, WA, USA, both in electrical engineering. In 1991, he was with Adelaide University, Adelaide, Australia. In 1998, he was an Associate Professor with Edith Cowan University, Perth, Australia. In 2004, he was a Professor with the Department of Computer Engineering, University of Wollongong, and the Head of School of Electrical, Computer and Telecommunications Engineering. Since 2007, he has been an Associate Dean (Research) with the Faculty of Informatics. He held a number of Visiting Appointments at several Universities and research Institutes, including Institut Galilée, Université Paris 13, LAAS-CNRS, Toulouse, France, the Hong Kong University of Science and Technology, Hong Kong, and Villanova University, Villanova, PA, USA. From 2009 to 2011, he served as a member of the Australian Research Council College of Experts and was the Deputy Chair of the EMI panel from 2010 to 2011.

He has received numerous awards and prizes; most notable are the Eureka Prize for Outstanding Science in Support of Defense or National Security in 2011, the Chester Sall Award in 2005, and a Distinguished Researcher Award from the French Ministry of Research in 2001. He has published over 280 technical articles and graduated many Ph.D. and Masters students. From 1999 to 2006, he served as an Associate Editor of the IEEE TRANSACTIONS SYSTEMS, MAN AND CYBERNETICS. He is currently an Associate Editor of three international journals and a member of the Governing Board of the Asia Pacific Neural Network Assembly. He is a member of OSA and INNS.

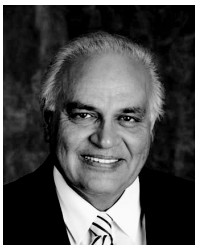

Moeness G. Amin (F'01) received the Ph.D. degree in electrical engineering from the University of Colorado, Boulder, CO, USA, in 1984. He has been the Faculty with the Department of Electrical and Computer Engineering, Villanova University, Villanova, PA, USA, since 1985. In 2002, he was the Director of the Center for Advanced Communications, College of Engineering. He is a recipient of the 2009 Individual Technical Achievement Award from the European Association of Signal Processing, the Recipient of the 2010 NATO Scientific Achievement Award, the Chief of Naval Research Challenge Award in 2010, the IEEE Third Millennium Medal in 2000, the Villanova University Outstanding Faculty Research Award in 1997, and the IEEE Philadelphia Section Award in 1997. He is a fellow of the International Society of Optical Engineering in 2007 and the Institute of Engineering and Technology in 2010. He was a Distinguished Lecturer of the IEEE Signal Processing Society from 2003 to 2004. He serves as the Chair of the Electrical Cluster of the Franklin Institute Committee on Science and the Arts. He has published over 600 journal and conference publications in the areas of Wireless Communications, Time-Frequency Analysis, Smart Antennas, Waveform Design and Diversity, Interference Cancellation in Broadband Communication Platforms, Anti-Jam GPS, Target Localization and Tracking, Direction Finding, Channel Diversity and Equalization, Ultrasound Imaging, and Radar Signal Processing. He is an Editor of *Through the Wall Radar Imaging* (CRC Press, 2011) and *Compressive Sensing for Urban Radar* (CRC Press, 2014).

Son Lam Phung (M'03) received the B.Eng. (Hons.) degree and the Ph.D. degree in computer engineering from Edith Cowan University, Perth, Australia, in 1999 and 2003, respectively. He received the University and Faculty Medals in 2000. He is currently a Senior Lecturer with the School of Electrical, Computer and Telecommunications Engineering, University of Wollongong, Wollongong, Australia. His general research interests are in the areas of image and signal processing, neural networks, pattern recognition, and machine learning.